NANO LETTERS

Letter

pubs.acs.org/NanoLett

Nanocathodoluminescence Reveals Mitigation of the Stark Shift in InGaN Quantum Wells by Si Doping

James T. Griffiths,*[,†] Siyuan Zhang,[†] Bertrand Rouet-Leduc,[†] Wai Yuen Fu,[†] An Bao,[†] Dandan Zhu,[†,‡] David J. Wallis,[†,‡] Ashley Howkins,[§] Ian Boyd,[§] David Stowe,[∥] Menno J. Kappers,[†] Colin J. Humphreys,[†] and Rachel A. Oliver[†]

[†]Department of Materials Science and Metallurgy, University of Cambridge, Charles Babbage Road, Cambridge CB3 0FS, United Kingdom

[‡]Plessey Semiconductors, Tamerton Road, Plymouth PL6 7BQ, United Kingdom

[§]Experimental Techniques Centre, Brunel University, Uxbridge UB8 3PH, United Kingdom

[∥]Gatan U.K., 25 Nuffield Way, Abingdon, Oxon OX14 1RL, United Kingdom

ABSTRACT: Nanocathodoluminescence reveals the spectral properties of individual InGaN quantum wells in high efficiency light emitting diodes. We observe a variation in the emission wavelength of each quantum well, in correlation with the Si dopant concentration in the quantum barriers. This is reproduced by band profile simulations, which reveal the reduction of the Stark shift in the quantum wells by Si doping. We demonstrate nanocathodoluminescence is a powerful technique to optimize doping in optoelectronic devices.

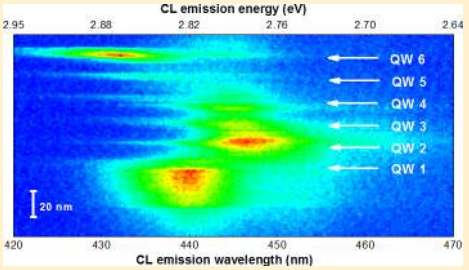

KEYWORDS: *Nanocathodoluminescence, scanning transmission electron microscopy, InGaN optoelectronics, light emitting diodes, quantum confined Stark effect, silicon doping*

High efficiency InGaN light emitting diodes (LEDs) have superior energy efficiency compared to traditional lighting leading to reductions in energy consumption and air pollutants including greenhouse gases.[1] Modern LEDs use multiple InGaN quantum wells (QW) with GaN quantum barriers (QB) between the QWs to confine the carriers and lead to high brightness devices, such as shown in Figure 1a. However, a persistent challenge to the development of higher efficiency devices is the presence of the strong polarization field across the QWs along the GaN polar axis [0001].[2,3] The polarization induced internal electric fields cause spatial separation of the electron and hole wave functions in the QWs,[4,5] known as the quantum confined Stark effect (QCSE). The QCSE results in a red-shift in the emission and reduced radiative recombination rates thus rendering the device less efficient. It has been proposed that the internal electric field can be suppressed by Si doping the QBs[6−8] and thus improve the device efficiency. The inclusion of a Si doped layer before the growth of the QWs has also been reported to improve the quantum efficiency.[9−12] Moreover, Kim et al.[13] have theoretically shown that to achieve the maximum device efficiency requires optimization of the Si dopant concentrations through the QWs.

To confirm the simulated properties it is crucial to resolve the spectral properties of individual QWs and the influence of dopants on the local emission and electric fields. However, common luminescence characterization techniques, such as electroluminescence (EL)[14] and photoluminescence (PL),[6,7] lack the spatial resolution to resolve emission from individual QWs. Cathodoluminescence (CL) in a scanning electron microscope (SEM) has finer spatial resolution than EL or PL and has been employed to correlate the luminescence characteristics with structural features. However, the spatial resolution is several tens of nanometers,[15−18] and a further improvement in spatial resolution is required to study the spectral properties of individual QWs.

Recently, by performing CL in a scanning transmission electron microscope (STEM), a CL spatial resolution of a few nanometers has been demonstrated by Zagonel et al.; an approach referred to as nano-CL.[19,20] Their nano-CL studies on GaN/AlN quantum discs have demonstrated a blue shift caused by quantum confinement for the first time on the same length scale as the device structure. Since then, nano-CL has been applied to study spectral properties of GaN quantum dots,[21] stacking faults in GaN nanocolumns,[22] InGaN insertions in nanowires,[23,24] and quasi-bulk InGaN.[25] Nano-CL is thus the only approach that can discern the local influence of dopants on the emission properties of individual InGaN QWs.

In this letter, we show for the first time the spectral properties of individual InGaN QWs in LEDs and reveal the influence of doping on the peak emission wavelength. Nano-CL

Received: September 2, 2015
Revised: October 19, 2015
Published: October 21, 2015

DOI: 10.1021/acs.nanolett.5b03531
Nano Lett. 2015, 15, 7639−7643

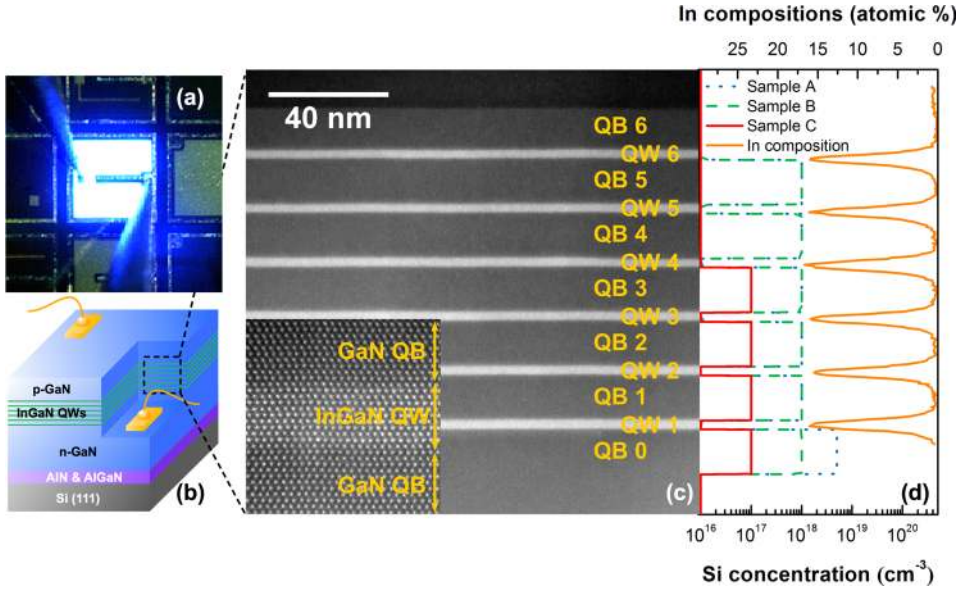

Figure 1. (a) Electroluminescence of a sample LED structure. (b) Schematic of the LED structure along with (c) the aberration-corrected HAADF-STEM image, with the QW/QB nomenclature and a magnified view of QW1. (d) The Si doping profile through the structures and the measured In composition profile.

is used to resolve the QCSE shifts of individual QWs and the suppression of the internal electric field by Si doping in different LED designs.

For this investigation, we study LED structures (samples A, B, and C) with varying Si dopant profiles across the active QW and QB region. All samples were grown by metal−organic vapor-phase epitaxy (MOVPE) and a schematic of the full device structure is shown in Figure 1b. A 200 nm AlN buffer layer was grown on a Si(111) substrate followed by the growth of a 600 nm graded AlGaN for stress management.[26] A 2 μm GaN layer was grown on top of the buffer layers. Six 3.0 nm InGaN QWs were grown separated by 14.7 nm GaN QBs. As illustrated in Figure 1c, scanning transmission electron microscope (STEM) images acquired in a probe aberration-corrected FEI Titan verifies that all QWs have uniform thicknesses, and the inset Figure 1c shows abrupt interfaces with the QBs. The In composition of each QW was measured by energy-dispersive X-ray spectroscopy (EDS) and confirms all six QWs are chemically indistinguishable $In_{0.17}Ga_{0.83}N$ (Figure 1d).

The Si doping profiles of each sample are summarized in Figure 1d. The Si doping profile of sample A was optimized in collaboration with Plessey Semiconductors, which includes a Si doped QB0 at a concentration of 5×10^{18} cm^{-3} with the following barriers QB1−5 doped at 1×10^{18} cm^{-3}. To study the influence of the higher QB0 doping, reference sample B was grown with constant QB doping 1×10^{18} cm^{-3} from QB0 to QB5. A second reference, sample C, was grown with 1×10^{17} cm^{-3} or less Si doping across the QBs.

Nano-CL experiments were performed on a JEOL 2100F Schottky field emission gun TEM fitted with a Gatan Vulcan CL system. Miniature elliptical mirrors are positioned above and below the specimen to provide a light collection angle of up to 7.2 sr. Spectral profiles were recorded by scanning a 0.2 nm electron probe across the active region. The CL, electron energy loss spectroscopy (EELS), and high angle annular dark field (HAADF) signals were recorded every 1 nm, to provide simultaneous luminescent and structural information. An 80 keV electron probe energy was used to enhance the luminescent intensity and minimize specimen damage. The samples were prepared by mechanical polishing followed by Ar^+ ion milling at 5 keV, with a final 1 keV polish.

Figure 2 shows a spectral CL profile across the QW/QB of sample A, along with the HAADF intensity and EELS plasmon peak energy profiles. Non-negative matrix factorization based multivariate analysis[27] was applied to the CL spectral line profiles to improve the signal-to-noise ratio of the CL spectra. A Gaussian profile was fitted to each CL spectrum along the line profile to determine the peak emission wavelength. We

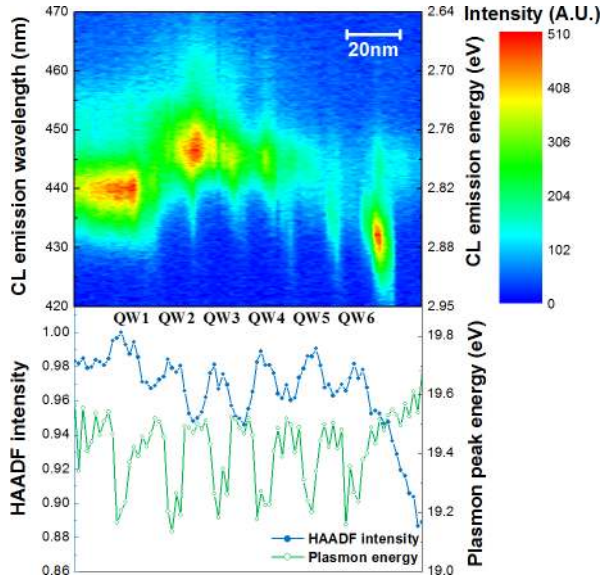

Figure 2. CL spectral profile across the InGaN/GaN QWs of sample A, scanned from QW1 to QW6 recorded every 1 nm, with a dwell time of 0.5 s and 5 nm spectrometer bandpass. The simultaneously recorded HAADF intensity profile (InGaN is higher than GaN) and EELS plasmon peak energy position profile (InGaN is lower than GaN) are displayed below.

DOI: 10.1021/acs.nanolett.5b03531
Nano Lett. 2015, 15, 7639−7643

observe six distinct spectral features that relate to QW1−6, whose positions were identified by the simultaneously recorded HAADF intensity and EELS plasmon peak energy position profiles (Figure 2). The spatial separation of the CL spectral features is finer than the QW/QB period of ∼18 nm, which is significantly smaller than the resolution limit set by the carrier diffusion length, ∼100 nm for GaN and InGaN.[28−30] The quantum confinement of carriers within the QW leads to the observed improvement in CL spatial resolution.[19]

The demonstrated fine spatial resolution of nano-CL has shown the emission of individual QWs and revealed a variation in the peak emission wavelength across the individual QWs of sample A, despite being chemically and structurally identical. We quantitatively study the variation in the emission peak wavelength of each QW by recording 20 line profiles for statistical reliability, scanned both from QW1 to QW6 and in the reverse direction. The mean emission wavelength of each QW and its variance (1−2 nm) are plotted in Figure 3 for all

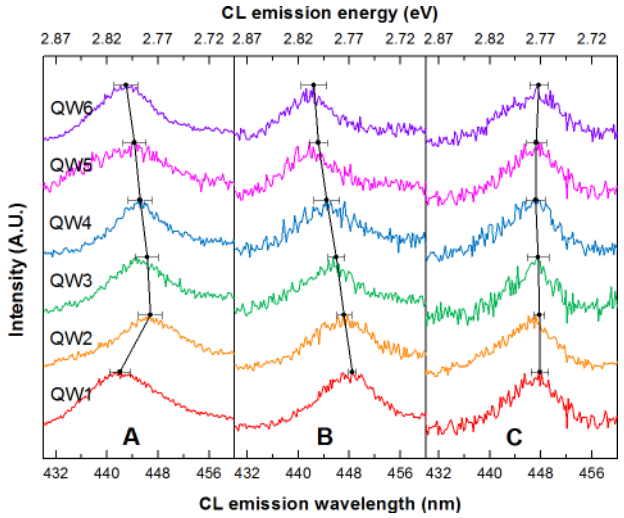

Figure 3. Mean emission wavelength and the standard deviation from 20 spectral line profiles of samples A, B, and C, superimposed on the CL spectra from the center of each individual QW.

three samples. The normalized CL spectra at the center of each QW are superimposed on Figure 3. We observe in reference sample C with 10^{17} cm^{-3} doping a negligible shift (<1 nm) in the emission wavelength between QWs. This confirms that there is no major factor other than Si doping that causes the variation in the emission wavelength between QWs. For sample B, as the Si doping is increased to 10^{18} cm^{-3}, a constant blueshift in the emission wavelength from QW1 to QW6 is observed. Sample A also shows a constant blueshift from QW2 to QW6, as is seen in sample B. The increased Si doping of QB0 in sample A induces a blueshift in the peak emission of QW1 with respect to QW2, in contrast to sample B.

To understand the correlation between the Si doping and the variation in emission wavelengths, electronic band profile simulations of the experimental structures are performed using the Crosslight APSYS simulation package. Materials parameters were taken from the text by J. Piprek.[31] The band structure was calculated using the 6 × 6 k·p method[32] in a finite volume approximation. The carrier transport equations were self-consistently computed and coupled with the Schrödinger equation to determine the confined states in the QWs. Schrödinger and Poisson equations were solved iteratively to account for the band structure deformation with carrier redistribution. We use the literature values for the ionization energy of Si in GaN (20 meV), as well as a 50% activation fraction.[33−35] Simulations were performed at zero bias, corresponding to the state examined during nano-CL experiments.

Figure 4a shows the simulated emission wavelengths of each QW accurately reproduce the variations in the emission wavelength of all three samples within the experimental errors. The simulated electric field at the center of each QW shown in Figure 4b shows the same trend observed in the emission wavelength. The mitigation of the QCSE solely explains the observed variation in emission wavelength between each QW and reflects the difference in the local electric field at each QW. We observe that the electric field is uniform across the QWs in sample C with up to 10^{17} cm^{-3} Si doping in the QBs. With 10^{18} cm^{-3} Si doping introduced in samples A and B the electric field is reduced toward QW6. An additional reduction in the electric field of QW1 is seen in sample A, with the higher level of doping in QB0. The additional reduction in the electric field of QW1 results in a more constant emission wavelength across the QWs of sample A, with a narrower range of emission wavelengths in contrast to sample B. Among the three structures, sample A shows the lowest overall electric field and strongest mitigation of the QCSE.

To understand the observed variation in emission wavelength and electric field between QWs, the simulated band profiles, charge concentrations, and electric field of sample A are shown in Figure 4c−e. Figure 4d shows the polarization charges are localized at the interfaces between the QW and QB and have the same magnitude across all QWs as they only depend on the QW width and composition. The Si^+ concentration is significantly higher in QB0 due to the increased doping concentration there. Figure 4c shows that the conduction band rises from QW1 to QW6 with respect to the Fermi level in response to the QB doping and subsequent charge redistribution and hence the free electron concentration decreases from QW1 to QW6 (Figure 4d). The hole concentrations are negligible as the Fermi level is significantly higher than the valence band.

Figure 4e shows the electric fields induced by the polarization charges, Si^+, and the free electrons, calculated by the integration of the respective charge concentrations over the position along the growth axis. The electric field induced by polarization charges is −1.55 MeV/cm in each of the six QWs. The Si^+ electric field is of the opposite sign to the polarization field and hence mitigates the field. However, the electric field of the electrons enhances the polarization field.

The significantly higher Si^+ concentration in QB0 of sample A screens the electric field of QW1 and results in the observed blueshift of QW1 with respect to QW2. For sample B, the doping in QB0 is the same as in the subsequent QBs and hence we do not observe a blueshift of QW1 with respect to the subsequent QWs.

The observed reduction in the field over QW2 to QW6 of sample A arises from the reduction in the electron populations. The lower electron concentrations in QW3−6 do not enhance the polarization field as greatly as QW2, which leads to the observed gradual blueshift in the emission wavelength from QW2 to QW6. Likewise, the gradual blueshift from QW1 to QW6 seen in sample B is caused by the reduction in the electron populations from QW1 to QW6, while Si^+ remains the same for each QB. As the Si dopant level in the QBs falls below

DOI: 10.1021/acs.nanolett.5b03531
Nano Lett. 2015, 15, 7639−7643

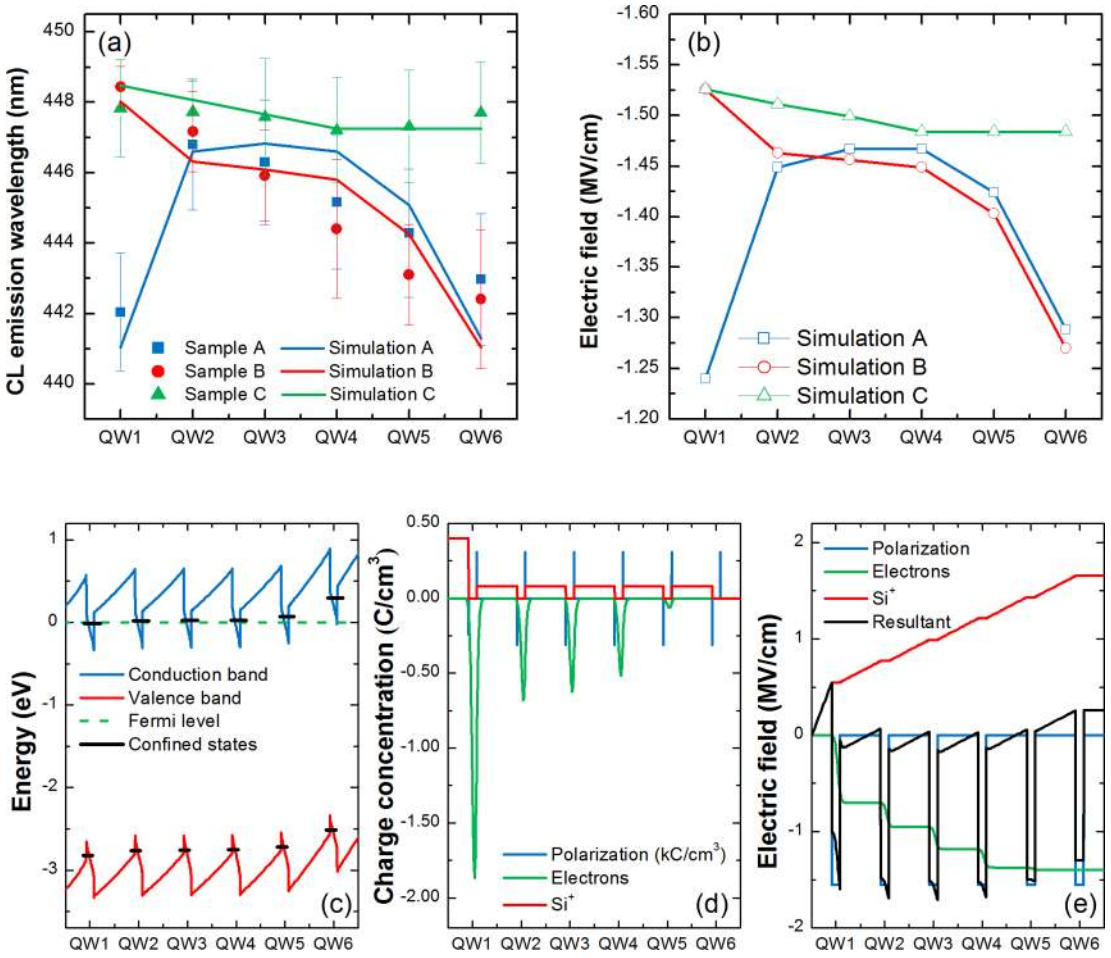

Figure 4. (a) Simulated variation in the emission wavelength across each QW, plotted with the experimental data. (b) Simulated variation in the internal electric field at the center of each QW. (c) Sample A equilibrium band profile showing the conduction and valence bands along with the ground state energy levels of the confined electron and hole states in the QW. (d) Concentration of polarization charges, electrons, and Si^+ dopants. (e) Electric field due to the polarization charges, electrons, Si^+ dopants, and the resultant electric field.

10^{17} cm^{-3} in sample C the conduction band energy remains constant across the QWs, and there is little variation in the electron populations through the QWs. Due to the constant electron populations through the QWs in sample C, there is no observed variation in the emission wavelength between QWs.

In conclusion, nano-CL has revealed the spectral properties of individual InGaN QWs and shown the mitigation of the QCSE in commercially designed InGaN multiple QW LEDs. We have observed variations in the emission wavelength, which correlate with the Si doping profile. We show that increases in the Si doping level leads to a reduction in the emission wavelength unique to the adjacent QW. Band profile simulations reproduce the experimental variations in the emission wavelengths and confirm the observed reduction in the emission wavelength is due to the mitigation of the QCSE. The three LED designs show different mitigation of QCSE in their QWs caused by their different doping profiles. The optimized design shows the overall highest degree of mitigation of the QCSE. Nano-CL can thus serve as an experimental approach to study and refine the design of future optoelectronic nanostructures, including the effects from doping and lead to greater improvements in device efficiencies and functionality. The fine spatial resolution and ability to simultaneously study the structural properties can further aid in the understanding of the emission properties of a wide range of nanostructures with quantum confinement, in the nitride community and beyond.

AUTHOR INFORMATION

Corresponding Author

*E-mail: jg641@cam.ac.uk.

Funding

This work was funded in part by the EPSRC (Grant no EP/J003603/1 and EP/H047816/1). The European Council has provided financial support under the European Community's Seventh Framework Programme (FP7/2007-2013) ERC grant agreement no. 279361 (MACONS).

Notes

The authors declare no competing financial interest.

REFERENCES

(1) Humphreys, C. J. *MRS Bull.* **2008**, *33*, 459−470.
(2) Fiorentini, V.; Bernardini, F.; Della Sala, F.; Di Carlo, A.; Lugli, P. *Phys. Rev. B: Condens. Matter Mater. Phys.* **1999**, *60*, 8849−8858.
(3) Bernardini, F.; Fiorentini, V.; Vanderbilt, D. *Phys. Rev. B: Condens. Matter Mater. Phys.* **1997**, *56*, R10024−R10027.
(4) Miller, D.; Chemla, D.; Damen, T.; Gossard, A.; Wiegmann, W.; Wood, T.; Burrus, C. *Phys. Rev. Lett.* **1984**, *53*, 2173−2176.
(5) Ren, C. *Mater. Sci. Technol.* **2015**, *00*, 1−16.

DOI: 10.1021/acs.nanolett.5b03531
Nano Lett. 2015, 15, 7639−7643

(6) Deguchi, T.; Shikanai, A.; Torii, K.; Sota, T.; Chichibu, S.; Nakamura, S. *Appl. Phys. Lett.* **1998**, *72*, 3329−3331.
(7) Cho, Y.-H.; Song, J. J.; Keller, S.; Minsky, M. S.; Hu, E.; Mishra, U. K.; DenBaars, S. P. *Appl. Phys. Lett.* **1998**, *73*, 1128−1130.
(8) Dalfors, J.; Bergman, J. P.; Holtz, P. O.; Sernelius, B. E.; Monemar, B.; Amano, H.; Akasaki, I. *Appl. Phys. Lett.* **1999**, *74*, 3299−3301.
(9) Akasaka, T.; Gotoh, H.; Saito, T.; Makimoto, T. *Appl. Phys. Lett.* **2004**, *85*, 3089−3091.
(10) Otsuji, N.; Fujiwara, K.; Sheu, J. K. *J. Appl. Phys.* **2006**, *100*, 113105−113107.
(11) Takahashi, Y.; Satake, A.; Fujiwara, K.; Shue, J.; Jahn, U.; Kostial, H.; Grahn, H. *Phys. E* **2004**, *21*, 876−880.
(12) Davies, M. J.; Dawson, P.; Massabuau, F. C.-P.; Fol, A.; Oliver, R. A.; Kappers, M. J.; Humphreys, C. J. *Phys. Status Solidi B* **2015**, *252*, 866−872.
(13) Kim, D. Y.; Lin, G.-B.; Hwang, S.; Park, J. H.; Meyaard, D.; Schubert, E. F.; Ryu, H.-Y.; Kim, J. K. *IEEE Photonics J.* **2015**, *7*, 1−9.
(14) Park, E.-H.; Kang, D. N. H.; Ferguson, I. T.; Park, S.-K.; J, J.-S.; Yoo, T.-K. *Appl. Phys. Lett.* **2007**, *90*, 031102.
(15) Petrov, V. I.; Gvozdover, R. S. *Scanning* **1991**, *13*, 410−414.
(16) Sonderegger, S.; Feltin, E.; Merano, M.; Crottini, A.; Carlin, J. F.; Sachot, R.; Deveaud, B.; Grandjean, N.; Ganière, J. D. *Appl. Phys. Lett.* **2006**, *89*, 232109.
(17) Lim, S. K.; Brewster, M.; Qian, F.; Li, Y.; Lieber, C. M.; Gradecak, S. *Nano Lett.* **2009**, *9*, 3940−3944.
(18) Merano, M.; Sonderegger, S.; Crottini, A.; Collin, S.; Renucci, P.; Pelucchi, E.; Malko, A.; Baier, M. H.; Kapon, E.; Deveaud, B.; Ganière, J.-D. *Nature* **2005**, *438*, 479−482.
(19) Zagonel, L. F.; Mazzucco, S.; Tencé, M.; March, K.; Bernard, R.; Laslier, B.; Jacopin, G.; Tchernycheva, M.; Rigutti, L.; Julien, F. H.; Songmuang, R.; Kociak, M. *Nano Lett.* **2011**, *11*, 568−573.
(20) Zagonel, L. F.; Rigutti, L.; Tchernycheva, M.; Jacopin, G.; Songmuang, R.; Kociak, M. *Nanotechnology* **2012**, *23*, 455205.
(21) Schmidt, G.; Müller, M.; Bertram, F.; Veit, P.; Petzold, S.; Das, A.; Monroy, E. *Microsc. Microanal.* **2012**, *18*, 1878−1879.
(22) Urban, A.; Müller, M.; Karbaum, C.; Schmidt, G.; Veit, P.; Malindretos, J.; Bertram, F.; Christen, J.; Rizzi, A. *Nano Lett.* **2015**, *15*, 5105−5109.
(23) Zhou, X.; Lu, M.-Y.; Lu, Y.-J.; Jones, E. J.; Gwo, S.; Gradečak, S. *ACS Nano* **2015**, *9*, 2868−2875.
(24) Tourbot, G.; Bougerol, C.; Glas, F.; Zagonel, L. F.; Mahfoud, Z.; Meuret, S.; Gilet, P.; Kociak, M.; Gayral, B.; Daudin, B. *Nanotechnology* **2012**, *23*, 135703.
(25) Pantzas, K.; Patriarche, G.; Troadec, D.; Kociak, M.; Cherkashin, N.; Hÿtch, M.; Barjon, J.; Tanguy, C.; Rivera, T.; Suresh, S.; Ougazzaden, A. *J. Appl. Phys.* **2015**, *117*, 055705.
(26) Zhu, D.; Wallis, D. J.; Humphreys, C. J. *Rep. Prog. Phys.* **2013**, *76*, 106501.
(27) Wang, Y.-X.; Zhang, Y.-J. *IEEE Trans. Knowl. Data Eng.* **2013**, *25*, 1336−1353.
(28) Yablonskii, G. P.; Gurskii, A. L.; Pavlovskii, V. N.; Lutsenko, E. V.; Zubialevich, V. Z.; Shulga, T. S.; Stognij, A. I.; Kalisch, H.; Szymakowski, A.; Jansen, R. H.; Alam, A.; Schineller, B.; Heuken, M. *J. Cryst. Growth* **2005**, *275*, e1733−e1738.
(29) Duboz, J.; Binet, F.; Dolfi, D.; Laurent, N.; Scholz, F.; Off, J.; Sohmer, A.; Briot, O.; Gil, B. *Mater. Sci. Eng., B* **1997**, *50*, 289−295.
(30) Chichibu, S.; Wada, K.; Nakamura, S. *Appl. Phys. Lett.* **1997**, *71*, 2346−2348.
(31) Piprek, J., Ed. *Nitride Semiconductor Devices: Principles and Simulation*; Wiley-VCH Verlag GmbH & Co. KGaA: Weinheim, Germany, 2007.
(32) Chuang, S. *Phys. Rev. B: Condens. Matter Mater. Phys.* **1991**, *43*, 9649−9661.
(33) Eiting, C. J.; Grudowski, P. A.; Dupuis, R. D.; Hsia, H.; Tang, Z.; Becher, D.; Kuo, H.; Stillman, G. E.; Feng, M. *Appl. Phys. Lett.* **1998**, *73*, 3875−3877.
(34) Irokawa, Y.; Fujishima, O.; Kachi, T.; Nakano, Y. *J. Appl. Phys.* **2005**, *97*, 083505.
(35) Hager, C. E.; Jones, K. A.; Derenge, M. A.; Zheleva, T. S. *J. Appl. Phys.* **2009**, *105*, 033713.

DOI: 10.1021/acs.nanolett.5b03531
Nano Lett. 2015, 15, 7639−7643